Cite this as: Inorg. Chem. 2021, 60, 11129–11139 **DOI: https://doi.org/10.1021/acs.inorgchem.1c01070**

Carboxylate Decorated Aggregation of Octanuclear Co_4Ln_4 (Ln = Dy, Ho, Yb) Complexes from Ligand Controlled Hydrolysis: Syntheses, Structures, and Magnetic Properties

*Mousumi Biswas,[a] E. Carolina Sañudo[b,c] and Debashis Ray[a,]**

[a]Department of Chemistry, Indian Institute of Technology, Kharagpur 721302, India

[b]Departament de Química Inorgànica i Orgànica, Universitat de Barcelona, Diagonal 645, 08028 Barcelona SPAIN

[c]Institut de Nanociència i Nanotecnologia, Universitat de Barcelona, (IN2UB) 08028 Barcelona SPAIN

ABSTRACT. One-pot separate reactions of an asymmetric carboxy-ether-phenol based Schiff base H_2L (2-((2-hydroxy-3-methoxybenzylidene)amino)benzoic acid) with selected $Ln(NO_3)_3{\cdot}nH_2O$ and $[Co_2(\mu\text{-}OH_2)(O_2CCMe_3)_4(HO_2CCMe_3)_4]$ (**Co_2-Piv**) in basic MeOH medium resulted in a family of three octanuclear complexes, $[Co^{II}_4Ln^{III}_4L_4(\mu_{1,3}\text{-Piv})_4(\mu_{1,1,3}\text{-Piv})_2(\eta^1\text{-Piv})_2(\mu_3\text{-OH})_4(MeOH)_2]{\cdot}mMeOH{\cdot}nH_2O$ (Ln = Dy; m=3, n=1 (**1**), Ho; m=4, n=0 (**2**), Yb; m=3, n=1 (**3**)). The options for incorporating different 4f ions in synthesis, without altering the actual metallic core structure, were successful for the three complexes. Single-crystal X-ray diffraction studies revealed that they are isostructural and built from two initially formed partial dicubane type $\{Co_2Ln_2L_2\}$ units. In each tetranuclear part the metal centres are held together by two L^{2-}, two μ_3-HO^-, three Piv^- bridges, one terminal Piv^- and one MeOH. The L^{2-} provides adjacent ONO and OO binding pockets ideal for selective coordination of bivalent cobalt and trivalent 4f ions. Four carboxylate ends of four L^{2-} units are responsible to connect two Co_2Ln_2 units into octanuclear structures. The unique distortion about the Co^{II} center is presented by the coordination of 4f metal ions at the hard OO coordination site. The distortion is further supported by the presence of COO^- groups on the ligand backbone and engaged in inter-tetrameric interactions. The dc magnetic susceptibility data revealed ferromagnetic coupling between the Co^{II} and Ln^{III} centers. Ac magnetic susceptibility measurements showed that complex **1** having highly anisotropic Dy^{III} ion behave as a single-molecule magnet (SMM) in absence of external magnetic field, with an energy barrier U_{eff} of 12.5 K.

Cite this as: Inorg. Chem. 2021, 60, 11129–11139 DOI: https://doi.org/10.1021/acs.inorgchem.1c01070

Introduction

Synthesis and comprehensive characterization of multinuclear trivalent lanthanide ion based aggregates with bi- or trivalent transition metal ions as neighbor has received considerable attention in recent times. The research endeavors not only provided intricate and aesthetically pleasing molecular structures but also face enormous synthetic challenges while providing interesting physical properties and applications.[1-7] These 3d-4f coordination aggregates (CAs) bearing 3d and 4f ions as near neighbors are of interest during the last two decades for their expected SMM behavior to show slow paramagnetic relaxation and hysteresis.[8-12] In recent years, synthesis of such molecular magnets showed potential in high-density magnetic data storage,[13] spintronics,[14-16] quantum computing,[17-19] and magnetic refrigeration.[20-22] The SMM complexes show facile quantum tunneling mechanism which shortcuts the effective relaxation energy barrier and thereby making them to lose magnetization very quickly. Hence for the goal of obtaining better SMMs, combination of 3d and 4f ions within a ligand frame and clipping them through appropriate donor atom bridges can be an advantageous process as the intermediate 3d–4f exchange interaction can significantly mitigate this quantum tunneling of magnetization (QTM) and improve the energy barrier for spin reversal.[23,24] The lanthanide ion present in these types of complexes have large ground spin state (S) and large anisotropy (D) due to its intrinsic single ion Ising type magnetic anisotropy, which can mediate ferromagnetic coupling.

Axially symmetric crystal-field around the 4f ions and strong exchange coupling between paramagnetic centers usually promotes the SMM behavior.[25,26] Co^{II} is a Kramers ion (S = 3/2) and the anisotropy in most six-coordinate octahedral Co^{II} complexes is generated from large and positive D values.[27] Many of the 4f ions exhibit strong magnetic anisotropy, such as Tb^{III} ($^7F_6$), Dy^{III} ($^6H_{15/2}$), and Ho^{III} ($^5H_8$), thus can be incorporated for the development of new Co^{II}-4f coordination aggregates expected to show SMM properties. Processes like fast QTM are usual for Co(II) and the lanthanoid ions, which can promote through-the-barrier fast relaxations.[28-30] The quenching of QTM is important to obtain better SMMs.[31,32] Hence the use of combined Co(II)-4f ions has as a goal to increase the energy barrier (U_{eff}) and magnetic blocking temperature (T_B) to show reasonably good SMM behaviour.[33,34] This is not always achieved and since the collinearity of anisotropy axes on the 4f ion in a polynuclear molecule is difficult to control, but it is necessary to garner the compound with strong axial anisotropy required for SMMs.[35]

The trivalent 4f ions are hard Lewis acids and show strong affinity for ligands having hard O-donors and ancillary bridges like HO^- and O^{2-}.[36-38] Thus hydrolytic reaction conditions can impose adventitious hydrolysis producing required numbers of hydroxide and oxide groups.[39-42] Choice of base and reaction medium is important to allow for the deprotonation of the lanthanide ion bound H_2O molecules followed by aggregation from the initially created ligand anion capped fragments. Thus, a rational approach for synthesis of HO^--bridged 3d-4f aggregates can contribute to a significant progress toward ligand-controlled hydrolysis and aggregation reactions. Carboxylates are also known as traditional ligands for lanthanide coordination, which can bind/bridge through varying mode favoring the incorporation of multiple numbers of 3d and 4f ions in any molecular aggregates in the presence of externally added or *in situ* generated hydroxide ions for the final product formation.[42,43-49]

The biggest synthetic challenge thus lies on the ligand design to arrest the outcome of the chosen reaction protocol. Standardization of the best reaction condition is of paramount importance to obtain 3d-4f aggregates of new structure. The procedure quite often follows the serendipitous and spontaneous self-assembly path because the outcome of that particular reaction path is unknown to the researchers by controlling/managing the hydrolysis. Thus, we expect a rich structural diversity in 3d-4f complexes compared to only transition metal ion bearing aggregates. In case of 3d ions the propensity for generation of several hydroxido and oxido linkers amongst multiple metal ions is low. The presence of ligand anion bound 3d ions can provide appropriate crystal fields to the 4f ions and the required anisotropy to see SMM properties. Fine-tuning and control of the anisotropy of such high nuclearity complexes are difficult to achieve through synthetic manipulations.

Herein, the asymmetric carboxy-ether-phenol based ligand 2-((2-hydroxy-3-methoxybenzylidene)amino)benzoic acid (H_2L) (Chart I) was synthesized to discover its synergistic metal ion binding capacity for new family of Co^{II}–4f coordination aggregates. Previously H_2L was explored for the reactions with dysprosium chloride and nitrate salts for Dy_4 and Dy_8 complexes from the assembly of as many as four and ten HL^- ions respectively.[50] In another work hydrothermal condition was utilized for $Na_2Ln_6L_8$ (Ln = Dy, Tb, Gd, Sm) complex.[51] Assembly of four L^{2-} ions around two M(II) and two Dy(III) ions provided one-dimensional ladder like double helical chain structures in $M_2Dy_2L_4$ complexes (M = Ni, Co).[52] Contrary to these findings our attempts following a new synthesis protocol instead provided a new family of octanuclear (4+4) $Co_4Ln_4L_4$ aggregates having *bis*-

partial-dicubane structures decorated and stabilized by several pivalate (Piv^-) groups.

Chart I. ChemDraw of H_2L showing two coordination bites

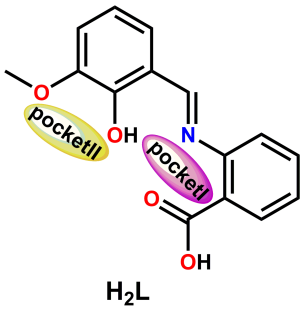

Composition of the resulting multimetallic aggregates were established as $[Co^{II}_4Ln^{III}_4L_4(\mu_{1,3}\text{-}Me_3CCOO)_4(\mu_{1,1,3}\text{-}Me_3CCOO)_2(\eta^1\text{-}Me_3CCOO)_2(\mu_3\text{-}OH)_4(MeOH)_2]\cdot mMeOH\cdot nH_2O$ (Ln = Dy; m=3, n=1 (**1**), Ho; m=4, n=0 (**2**), Yb; m=3, n=1 (**3**)). Two types of bridging coordination were achieved from terminal carboxy end of four L^{2-} which is responsible for the higher degree of aggregation (Scheme 1).

Scheme 1. Varying binding modes of carboxy ends L^{2-} observed in this work

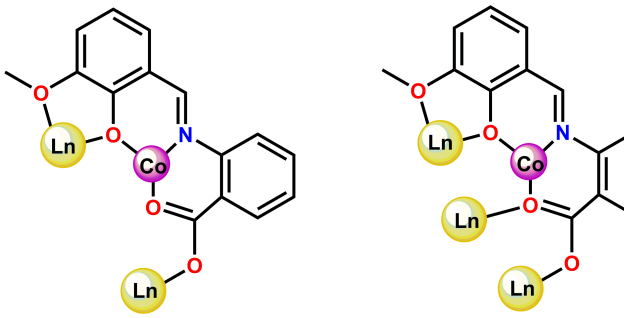

Experimental section

Reagents and Starting Materials. All the solvents and the reagents, were obtained from commercial sources and used as received without further purification. The following were used as obtained: $Dy(NO_3)_3\cdot 5H_2O$, $Ho(NO_3)_3\cdot 5H_2O$ and $Yb(NO_3)_3\cdot 6H_2O$ (Alfa Aeser, UK); $CoCO_3$ (SD Fine Chemicals, Mumbai, India); pivalic acid, 2-aminobenzoic acid, *o*-vanillin (Spectrochem Pvt. Ltd., Mumbai, India). Gram scale synthesis of **Co_2-Piv** was achieved following a known procedure.[53] Cobalt carbonate (4.0 g, 34mmol) and excess of pivalic acid (20.0 g, 196mmol) in presence of small amount of water (3 mL) was refluxed for 24 h at 100°C for the complete dissolution of the carbonate salt. Next, the solution was cooled to room temperature and 50 mL MeCN was added on rigorous stirring condition. The solution was then filtered and cooled to 5°C to produce pink coloured block shaped crystals which were washed with cold MeCN and dried in air. Yield = 67.2 %. The Schiff base H_2L was obtained following previously reported literature procedures of the condensation of *o*-vanillin and 2-aminobenzoic acid in a 1:1 molar ratio in MeOH (Scheme 2) and used as liquid.[54] Selected FT-IR peaks (KBr disc, cm^{-1}, vs = very strong, s = strong, m = medium, b = broad): 3364 (br), 2942 (br), 1671 (s), 1615 (vs), 1591 (s), 1486 (s), 1457 (m), 1369 (m), 1234 (vs), 1161 (m), 1067 (m), 1023 (m), 755 (m), 731 (m).

Scheme 2. Imine condensation for H_2L

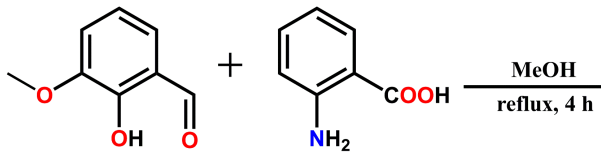

General synthetic routes for 1, 2, and 3. The complexes **1–3** were obtained following a general synthetic protocol. To H_2L (1 mL, 0.1mmol) solution in MeOH, $Ln(NO_3)_3{\cdot}nH_2O$ (n= 5, Dy, Ho; 6, Yb) (0.1mmol) in 2 mL MeOH and NEt_3 (55.6 µL, 0.4mmol) were added to obtain a clear solution. After 1 h of stirring at room temperature, **Co_2-Piv** (0.0474 g, 0.05mmol) in 2 mL MeOH was added dropwise producing a faint precipitate. The resulting orange reaction mixture was finally refluxed for 5 h at 70–80ºC. Filtrate obtained from the reaction mixture was kept for slow evaporation of solvent to obtain X-ray diffraction quality rhombus shaped orange crystals after 3 days.

*$[Co_4Dy_4L_4(\mu_{1,3}\text{-}Me_3CCOO)_4(\mu_{1,1,3}\text{-}Me_3CCOO)_2(\eta^1\text{-}Me_3CCOO)_2(\mu_3\text{-}OH)_4(MeOH)_2]{\cdot}H_2O{\cdot}3MeOH$ (**1**)*. The following reagents were used: H_2L (1 mL, 0.1mmol), $Dy(NO_3)_3{\cdot}5H_2O$ (0.0438 g, 0.1mmol), **Co_2-Piv** (0.0474 g, 0.05mmol), NEt_3 (55.6 µL, 0.4mmol). Yield: 0.037 g, 49 % (based on Dy). Anal. Calcd for $C_{105}H_{142}Co_4Dy_4N_4O_{42}$ (3017.92 g mol^{-1}): C, 41.79; H, 4.74; N, 1.86. Found: C, 41.63; H, 4.68; N; 1.75. Selected FTIR peaks (KBr, cm^{-1}; s = strong, vs = very strong, m = medium, br = broad, w = weak): 2957 (br), 2927 (br), 1605 (s), 1552 (vs), 1483 (m), 1470 (m), 1457 (m), 1417 (s), 1388 (m), 1375 (m), 1358 (m), 1309 (m), 1230 (vs), 1194 (s), 1095 (m), 1075 (w), 973 (m), 858 (m), 769 (m), 736 (s), 601 (m), 585 (m), 555 (m).

*$[Co_4Ho_4L_4(\mu_{1,3}\text{-}Me_3CCOO)_4(\mu_{1,1,3}\text{-}Me_3CCOO)_2(\eta^1\text{-}Me_3CCOO)_2(\mu_3\text{-}OH)_4(MeOH)_2]{\cdot}4MeOH$ (**2**)*. $Ho(NO_3)_3{\cdot}5H_2O$ (0.0441 g, 0.1mmol) was used in place of $Dy(NO_3)_3{\cdot}5H_2O$ as in previous synthesis . Yield: 0.044 g; 57% (based on Ho). Anal. Calcd for $C_{106}H_{144}Ho_4Co_4N_4O_{42}$ (3041.68 g mol^{-1}): C, 41.86; H, 4.77; N, 1.84. Found: C, 41.79; H, 4.69; N; 1.81. Selected FTIR peaks (KBr, cm^{-1}; s = strong, vs = very strong, m = medium, br = broad): 2957 (br), 2924 (br), 1605 (vs), 1552 (vs), 1483 (m), 1470 (m), 1457 (m), 1417 (vs), 1388 (s), 1375 (m), 1358 (m), 1309 (m), 1233 (vs), 1194 (vs), 1095 (m), 1078 (m), 970 (m), 858 (m), 769 (m), 733 (vs), 601 (m), 582 (m).

*$[Co_4Yb_4L_4(\mu_{1,3}\text{-}Me_3CCOO)_4(\mu_{1,1,3}\text{-}Me_3CCOO)_2(\eta^1\text{-}Me_3CCOO)_2(\mu_3\text{-}OH)_4(MeOH)_2]{\cdot}H_2O{\cdot}3MeOH$ (**3**)*. $Yb(NO_3)_3{\cdot}6H_2O$ (0.0467 g, 0.1mmol) was used instead of $Dy(NO_3)_3{\cdot}5H_2O$. Yield: 0.040 g; 52% (based on Yb). Anal. Calcd for $C_{105}H_{142}Yb_4Co_4N_4O_{42}$ (3060.08 g mol^{-1}) C, 41.21; H, 4.68; N, 1.83. Found: C, 41.12; H,

4.75; N; 1.75. Selected FTIR peaks (KBr, cm^{-1}; s = strong, vs = very strong, m = medium, br = broad): 2953 (br), 2924 (br), 1605 (s), 1552 (vs), 1482 (m), 1470 (m), 1460 (m), 1417 (vs), 1388 (m), 1375 (m), 1358 (m), 1309 (m), 1233 (vs), 1194 (vs), 1095 (m), 1075 (m), 970 (m), 858 (m), 769 (m), 736 (s), 605 (m), 588 (m).

Physical Measurements. Elemental analysis (CHN) was performed by a PerkinElmer model 240C elemental analyzer. A Perkin Elmer Spectrum Two spectrometer was used to record the ATR-FTIR spectra by placing the samples over the ATR crystal. The phase purity of the compounds in the powder state was examined by powder X-ray diffraction (PXRD) patterns with a Bruker AXS X-ray diffractometer (40 kV, 20 mA) using Cu Kα radiation (λ = 1.5418 Å) within a 2θ range of 5–70° and a fixed-time counting of 4s at 25°C.

Magnetic Measurements. Magnetic measurements were carried out in the Unitat de Mesures Magnètiques (Universitat de Barcelona) on polycrystalline samples (*circa* 30 mg) with a Quantum Design SQUID MPMS-XL magnetometer equipped with a 5 T magnet. Diamagnetic corrections were calculated using Pascal's constants and an experimental correction for the sample holder was applied.

X-ray Crystallographic Measurements. The single crystal X-ray structures of the complexes **1-3** were measured on Bruker SMART APEX-II CCD X-ray diffractometer, equipped with a graphite monochromator of Mo-Kα radiation (λ = 0.71073 Å) by the ω scan (width of 0.3° $frame^{-1}$) method at 293 K with a scan rate of 6 s per frame. The program SMART[55] was used for collecting frames of data, indexing of reflections. The software XPREP was used to determine space group and SAINT was used for integration of data.[55] The empirical absorption corrections were applied to the data using the program SADABS.[56] The structures were solved by direct method using the SHELXS-2014[57] program and refined with full-matrix least-squares technique against F^2 using SHELXL-2014[58] program package in Olex-2.[59] The hydrogen atoms were fixed in calculated position and refined with fixed geometry and riding thermal parameters with respect to their carrier atoms. All the non-hydrogen atoms were refined anisotropically. The used crystallographic figures were generated using Mercury 3.1 and POV-ray software.[60] The information regarding X-ray refinement data is summarized in Table 1. Crystallographic data have been deposited with the Cambridge Crystallographic Data Centre as supplementary publications CCDC 2075692 (**1**), 2075693 (**2**) and 2075694 (**3**).

Results and Discussion

Design Strategy and Synthesis. Structurally pentadentate imine-centered and ether side group bearing ligand H_2L was obtained from direct Schiff base condensation reaction of 2-aminobenzoic acid and o-vanillin. Plan was made to reserve the tridentate imine pocket for coordination of Co^{II} ion and let the adjacent –OMe group attracts bigger lanthanide ions through 3d-4f bridging action of central phenolate group. In lieu of any simple cobalt(II) salt, use of **Co_2-Piv** was considered to adopt a different course of reaction with help of already bound pivalate anions to the cobalt(II) centers which may not possible through external addition of pivalate anions from outside after mixing of the initial ingredients. These cobalt bound pivalate anions help in a positive manner to grow the aggregate during bridging and scrambling for coordination of these carboxylate anions between the 3d and 4f ions. Thus stepwise reactions of H_2L with $Ln(NO_3)_3{\cdot}nH_2O$ (Ln = Dy, Ho, Yb) and **Co_2-Piv** followed by dropwise addition of NEt_3 in a particular (1:1:0.5:4) molar ratio in MeOH medium and long refluxing condition provided $[Co_4Ln_4L_4(\mu_{1,3}\text{-}Me_3CCOO)_4(\mu_{1,1,3}\text{-}Me_3CCOO)_2(\mu\text{-}Me_3CCOO)_2(\mu_3\text{-}OH)_4(MeOH)_2]{\cdot}$ $mMeOH{\cdot}nH_2O$ (Co = Co^{II}; Ln = Dy^{III} (**1**), Ho^{III} (**2**), Yb^{III} (**3**); (Scheme 3). In all three cases the complexes were isolated as single-crystalline materials and nice rhombus shaped orange-colored crystals were obtained after 3 days. The selected single crystals were next used for X-ray structure determinations. The spontaneous assembly reaction for the generation of the coordination aggregates **1–3** is summarized in eq 1.

$$\begin{aligned} 4H_2L + 4Ln(NO_3)_3 \cdot (5-6)H_2O + 2[Co_2(\mu &- OH_2)(O_2CCMe_3)_4(HO_2CCMe_3)_4] \\ &\rightarrow [Co_4Ln_4L_4\{\mu_{1,3} \\ &- (Me_3CCOO)\}_4\{\mu_{1,1,3} \\ &- (Me_3CCOO)\}_2\{\eta^1 \\ &- Me_3CCOO\}_2\{\mu_3 \\ &- OH)_4(MeOH)_2] \cdot mMeOH \cdot nH_2O \\ &+ 12NO_3^- + 8Me_3COOH + 12H^+ \\ &+ H_2O \end{aligned}$$

… (1)

The octanuclear (4+4) 3d-4f aggregates were produced from spontaneous and cooperative assembling of four L^{2-} units, around four cobalt and four chosen 4f metal ions, and both types have dissimilar coordination demands. The crystalline and pure solid products thus obtained from the above-mentioned reaction protocols were analyzed first by ATR-FTIR spectroscopy

Scheme 3. Synthetic route for complexes **1-3**

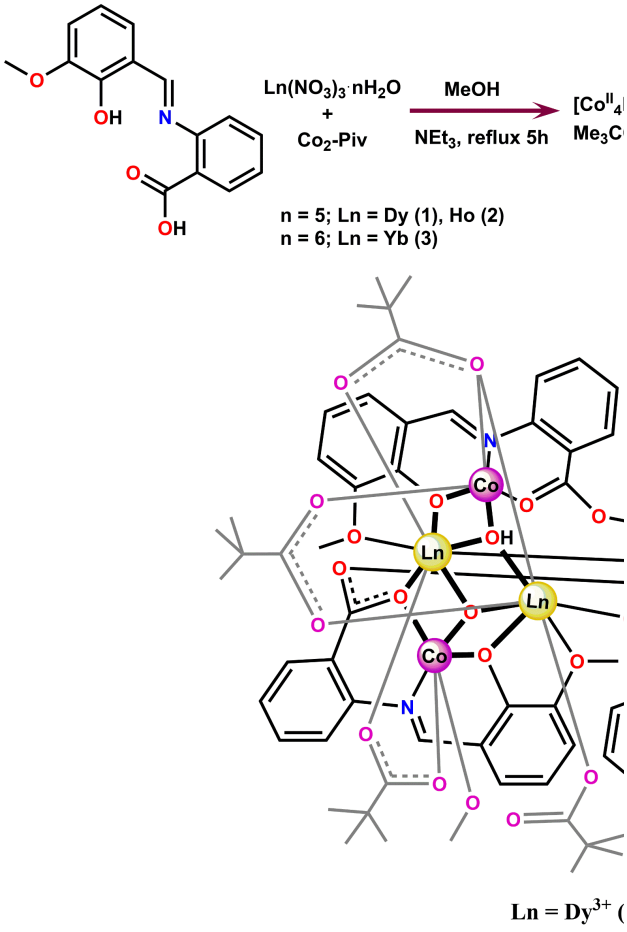

Ln = Dy^{3+} (

and PXRD patterns (Figures S1 and S2 in Supporting Information). The imine bond stretching vibration ($\tilde{\nu}_{C=N}$) is observed at 1603-1606 cm^{-1} confirming the binging of four Co^{II} ions by four L^{2-} through central imine N atom. The presence of multiple numbers of sterically bigger pivalate groups were identified from the asymmetric $\tilde{\nu}_{as(C=O)}$ bond stretching vibration at 1549-1552 cm^{-1} and the symmetric ($\tilde{\nu}_{sC=O}$) one at 1415-1417 cm^{-1} for **1–3**. The phase purity and the crystalline nature of the products from each synthetic attempt were confirmed by solid-state PXRD patterns, which showed good agreement of experimental peak positions with those of simulated versions from the single-crystal X-ray diffraction. The reproducibility of the PXRD patterns along with FTIR spectra were useful to identify and compare the products in each attempt.

Crystal Structure Descriptions. Suitable single crystals of **1–3** were directly obtained from the filtrate of the final reaction mixtures following slow evaporation of solvent in ambient conditions. All three electro-neutral complexes are found to be isostructural, and interestingly, all of them crystallize in same monoclinic system and space group, $P2_1/c$. In all cases, the entire structure appeared as a whole without the appearance of any smaller asymmetric fragment of the unit cell. However, smaller parts may be considered as the aggregating fragments involved in the growth of the whole structure.

All the three complexes are structurally similar and thus a complete description of structure for complex **1** (Ln = Dy^{III}) has been considered as a representative one for the whole family. Selected bond distances and bond angles are presented in Tables S3–S4 in the Supporting Information. The perspective view for dinuclear, tetranuclear fragments and the whole octanuclear aggregate of complex **1** is shown in Figure 1.

The analysis of the X-ray structure revealed that each L^{2-} unit (there are four such overall) binds one Co^{II} center in the imine pocket I also bears several pivalate anions obtained from **Co_2-Piv** used in the synthesis (Chart I). The available O,O donor part, consisting of the bridging phenoxido oxygen and adjacent –OMe of pocket II, was exclusively used to grab the bigger, hard and oxophilic Dy^{III} center. Thus, each L^{2-} accommodate one each of Co^{II} and Dy^{III} centers and further clipped by one solvent derived HO^- ion. Self-aggregation of four such units through terminal carboxylate end of L^{2-} and bridging Piv^- groups finally provided the double-dicubane core structure of **1**. The octanuclear Co_4Dy_4 magnetic core was grown from the stacking of one Co_2Dy_2 partial dicubane (Figure 2) over another, through four column-like supports of carboxylate ends of four L^{2-}. Eight Piv^- anions bound to four Co^{II} ions and four Dy^{III} ions and two terminal MeOH groups fulfil the varying coordination demands of individual metal ions.

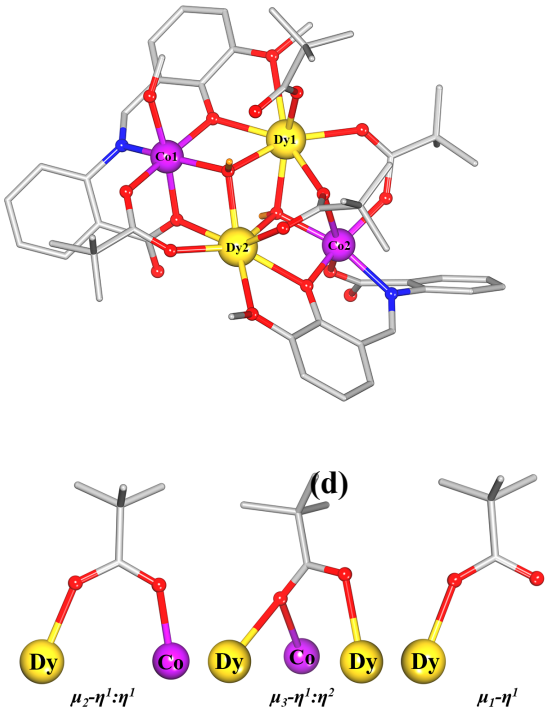

Figure 1. Retro structural analysis for (a) dimeric and (b) tetrameric fragments within **1**; (c) growth of octamer **1;** H atoms are shown for μ_3-OH groups only; (d) different binding modes of pivalate groups. Color code violet, Co^{II}; yellow, Dy^{III}; red, O; blue, N; grey, C; orange, H

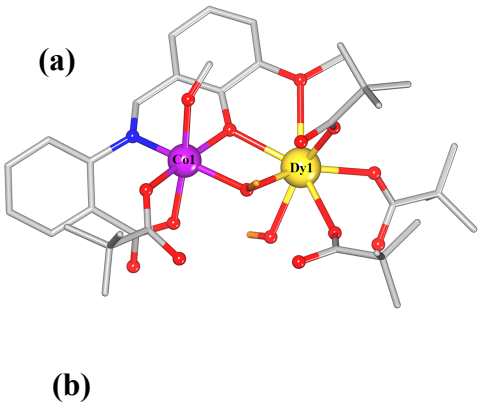

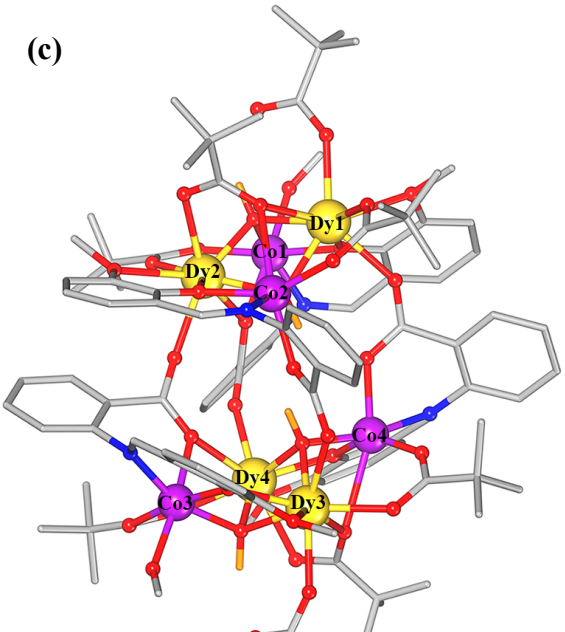

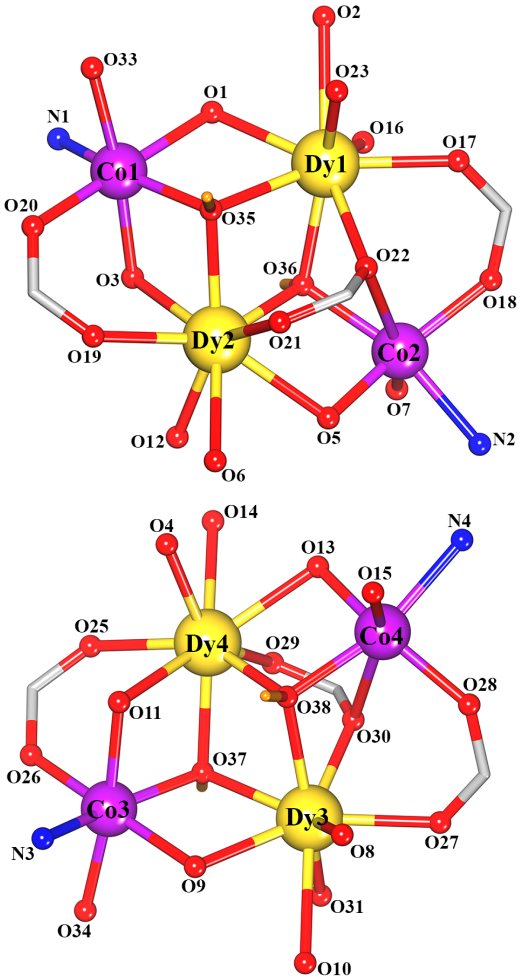

Figure 2. Atom connectivity within the two defective dicubane cores present in **1** with atom numbering scheme. Color codes as above

The eight-coordinate coordination geometry around Dy1 and Dy3 revealed distorted triangular dodecahedron structure (Figure 4a) as calculated from Continuous SHAPE Measures (CShM) by SHAPE 2.1.[61] The CShM of a molecular fragment is defined as its distance from an ideal shape, independent of size and orientation. Herein the measured value is close to the value for square antiprism structure (Table S1 in SI). Around Dy2 and Dy4 the shape is again distorted triangular dodecahedron (Figure 4b). Around Dy1 and Dy3 centers the eight coordination positions are assembled from O,OMe chelate part of L^{2-}, two μ_3-hydroxido, one $\mu_{1,3}$-pivalato bridge, one $\mu_{1,1,3}$-pivalato bridge, one monodentate pivalato group and one bridging carboxylato end of adjacent L^{2-}. Around Dy2 and Dy4 centers the eight coordination is fulfilled by one extra bridging carboxylato end of adjacent L^{2-} instead of one monodentate pivalate group. The Dy–O bonds span a considerable range of 2.299(6)–2.690(6) Å to result the distorted coordination environment with elastic bonding feature which is well matched to accommodate the bigger lanthanide ions. The longest length is thus achieved with coordination from –OMe end of L^{2-} to Dy^{III} centers, otherwise remain dangling as substitution on the ligand backbone, if appropriate coordination direction is not available. Water molecule derived two μ_3-OH nuclei were crucial to map the Co_2Dy_2 dicubane (defect) fragments. Within these units the Dy^{III} centers stayed at butterfly tips and form two Dy_2O_2 rhombuses having Dy···Dy separations of 3.661 Å and 3.685 Å. Where the Dy–O–Dy angles range from 102.30(19)° to 103.23(19)°, and O–Dy–O angles span the 73.94(17) to 75.53(18)° range. Within these Co_2Dy_2 units, showing considerable structural plasticity, four types of Co–O–Dy bond angles are detected within

88.16°–109.4(2)° range, resulting in eight different Co···Dy separations from 3.411 Å to 3.615 Å (Figure 3). The coordination from the other ends of the ligand carboxylate ends forces the aggregation of two such Co_2Dy_2 dicubane units through the formation of four new Dy–O bonds at 2.302(6)–2.396(6) Å.

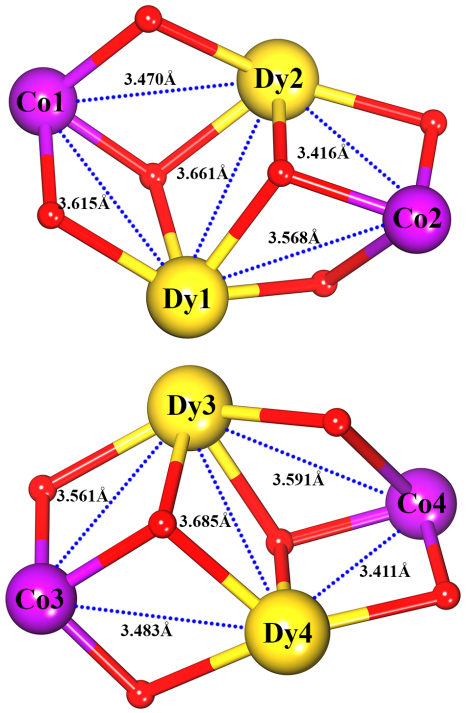

Figure 3. Different Dy···Dy and Co···Dy separations within the two different dicubane cores

The tridentate O,N,O half from carboxylate oxygen, imine nitrogen and phenoxido oxygen donors bind Co1, Co2, Co3 and Co4 centers in *facial* mode. A stressed arrangement of the ONO donor atoms on L^{2-} offered a severe distortion of the octahedral geometry around Co^{II} centers. The structural modification was achieved for an intermediate type, neither perfect *facial* nor *meridional* coordination of the ONO tridentate part to the Co^{II} center (Figure S4). Ancillary bridging support from μ_3-hydroxido, $\mu_{1,3}$ and $\mu_{1,1,3}$–pivalato groups, and terminal MeOH groups complete the Co_4Dy_4 core structure. Firm binding of the ligand anion resulted Co–N bonds within 2.109(8) to 2.148(7) Å. In octahedral coordination spheres around Co1 and Co3, the sixth coordination positions are occupied by terminal MeOH molecules. The dicubane site comprising Co1 and Co3 centers register O–Co–O and O–Co–N angles within a normal range of 77.4(2)°–99.7(3)° and 82.6(2)°–102.3(3)° confirming less distorted octahedral geometries (Figure 4c). Highly distorted octahedral geometry around Co2 and Co4 mainly arise from considerable elongation in Co–O bonds from 2.011(6) to 2.701 Å. Both six-coordinate Co2 and Co4 centers have distorted octahedral geometry (Shape Measures data in Table S2) with long Co–O bond (Co2–O22, 2.586 Å; Co4–O30, 2.701 Å) from oxygen donors of $\mu_{1,1,3}$-pivalato groups resulting unusually high magnitude of O–Co–N *cis* angles (O22–Co2–N2; O30–Co4–N4) of 120.90° and 121.80°. The complementary O–Co–O *cis* angles around Co2 and Co4 centers also suffered compression and elongation in 66.94°–109.6(2)° range. The Co^{II} centers within these aggregates had a natural preference for tetrahedral geometry thus could sustain

the huge distortion from neighboring Dy^{III} sites (Figure 4d). Both the chelate bites for coordination of L^{2-} anions to Co^{II} centers are six-membered. The amount of distortion is different for Co1 and Co3 compared to Co2 and Co4. In **1** the O–Co–N and O–Co–O angles from the binding of L^{2-} remain within 80.7(3)° to 109.6(2)° which are deviated from ideal angles for *facial* coordination. The NO_3 basal plane, in this orientation, is 21%, 32%, 20% and 33% distorted toward T_d (τ_4 is 0.21, 0.32, 0.20 and 0.33.) geometry. Monodentate coordination from –OMe group and bridging coordination *via* carboxylate end to bigger Dy^{III} centers further distort the bound ligand anion (L^{2-}) from a planar structure normally expected for considerable π-conjugation. For complex **1**, the amount of deviation is measured at 39.36°, 47.02°, 38.11° and 52.49° for the single L^{2-} anion with respect to the two phenyl rings present in the backbone of the ligand anion. Only one type

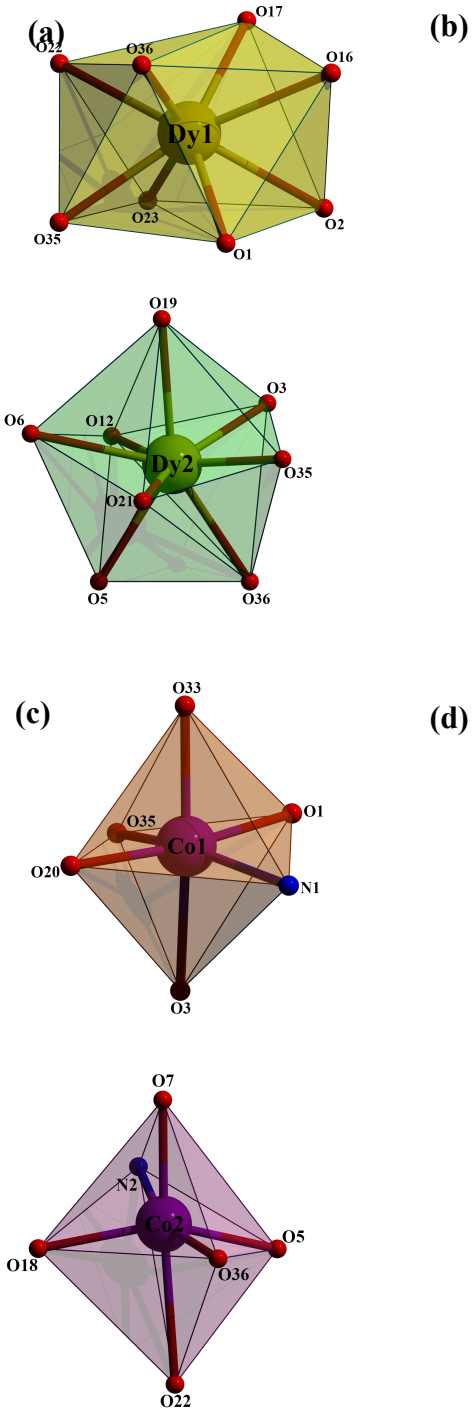

Figure 4. Four different coordination geometry around Dy1, Dy2, Co1 and Co2 in complex **1** (a) distorted triangular dodecahedron; (b) distorted triangular

dodecahedron; (c) distorted octahedron and (d) severely distorted octahedron

of double defect dicubane parts were formed during the initial stage of ligand-controlled aggregation. Within these $\{Ln_2O_2\}$ diamond cores the $Ln^{III}\cdots Ln^{III}$ separations follow the order **1** > **2** > **3** (Dy···Dy, 3.661 Å, 3.685 Å; Ho···Ho, 3.603 Å, 3.608 Å; Yb···Yb, 3.543 Å, 3.537 Å) due to the onset of lanthanide contraction across the series in trivalent states.

The entire structure experienced coordination of three different types of connectivity from pivalato anions solely originated from the **Co_2-Piv** salt. The connections from $\mu_{1,3}$-$Me_3CCO_2^-$ unit to Co^{II} and Dy^{III} centers provide shorter Co–O bonds at 2.011(6)–2.080(6) Å and longer Dy–O bonds at 2.310(6)–2.330(6) Å. The corresponding distances for $\mu_{1,1,3}$-$Me_3CCO_2^-$ bridges are slightly longer at 2.586–2.701 and 2.442(6)–2.467(6) Å. The terminal coordination from $Me_3CCO_2^-$ to Dy^{III} centers resulted shortest Dy–O bonds at 2.299(6) Å and 2.306(6) Å. These variations were crucial for the required adjustments in the metal ion and ligand donor atom separations. Likewise, carboxylato ends of L^{2-} provided $\mu_{1,3}$ and $\mu_{1,1,3}$ modes of bridging and expected bond distances for Co–O and Dy–O bonds.

Mean plane analysis for the coplanar arrangement of metal ions in Co_2Dy_2 parts revealed that the Dy^{III} centers remained 0.308-0.371 Å above and Co^{II} centers stayed 0.332-0.348 Å below this imaginary mean plane. Within the entire structure consisting of two such planes, the Dy^{III} ions remained above the plane with respect to the top one and stayed below with respect to latter (Figure 5).

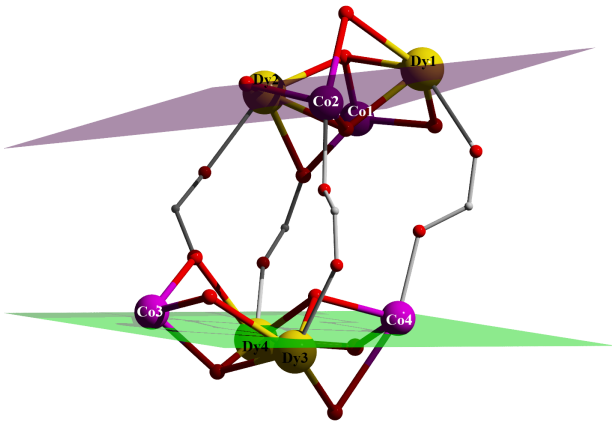

Figure 5. Orientation of two dicubane units with respect to the two mean planes. The rotation imposed by the ligands is clearly shown in this illustration.

Hydrogen bonding interactions involving μ_3–HO^- core bridging groups were important to maintain the secondary interactions for the stabilization of the grown crystals and crucial in holding the network structure in **1**. The μ_3–HO^- groups showed hydrogen bonds to the oxygen atoms of ligand carboxylato ends and other pivalate groups. Likewise, the μ_3–HO^- (O36 and O38) groups showed interactions with O15 and O7

(O36···O15, 2.867 Å; O38···O7, 2.882 Å) of ligand carboxylato donors. The other two μ_3–HO^- groups (O35 and O37) hydrogen bonded (O35···O24, 2.972 Å; O37···O32, 2.974 Å) to O24 and O32 of the pivalate anions already bound to Dy1 and Dy3. Further these pivalate oxygen (O24 and O32) donors engaged in hydrogen bond interactions with the O40 and O39 of MeOH solvent molecules (O24···O40, 2.893 Å; O32···O39, 2.813 Å) (Figure 6). Two such Co_4Dy_4 octamers showed inter molecular hydrogen bonding interaction with lattice MeOH (O41···O39, 2.641 Å).

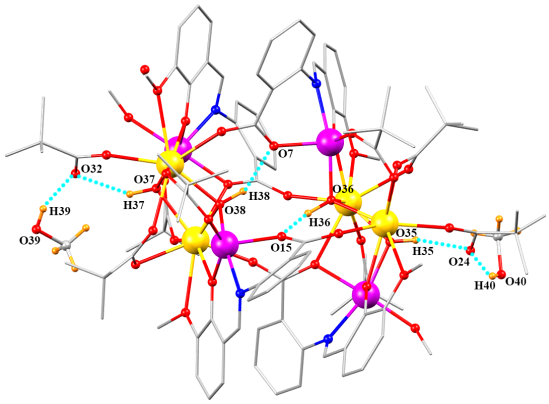

Figure 6. Intramolecular hydrogen bonding interactions in **1**

Table 1. Summary of crystallographic data and refinement parameters for **1–3**

	1 (Dy)	**2** (Ho)	**3** (Yb)
Empirical	$C_{105}H_{142}Co_4$	$C_{106}H_{144}Co_4$	$C_{105}H_{142}Co_4$
formula	$Dy_4N_4O_{42}$	$Ho_4N_4O_{42}$	$Yb_4N_4O_{42}$
Formula weight(g·mol^{-1})	3017.92	3041.68	3060.08
Crystal system	monoclinic	monoclinic	monoclinic
Space group	$P2_1/c$	$P2_1/c$	$P2_1/c$
a (Å)	29.919	29.607	29.157
b (Å)	16.360	15.931	15.799
c (Å)	26.979	26.598	26.258
β (°)	102.66	102.88	102.80
Volume (Å^3)	12884.8	12230	11795.3
Z	4	4	4
D_{calcd} (g cm^{-3})	1.555	1.652	1.722
Absorption coefficient t (mm^{-1})	2.868	3.166	3.770
F (000)	6024	6080	6088

Temperature(K)	299	293	298
Reflections collected/ unique	125064 / 27789	127831 / 26580	120937 / 27401
Parameters	1486	1488	1468
Index range	h = -38 → 38 k = -16 → 20 l = -34 → 34	h = -36 → 37 k = -19 → 20 l = -34 → 31	h = -38 → 35 k = -20 → 20 l = -32 → 34
Goodness-of-fit (F^2)	1.058	1.026	1.112
Largest diff peak/hole (e Å^{-3})	1.874, -1.169	0.952, -0.941	2.072, -1.327
R_{int}	0.0898	0.0787	0.0797
R1;	0.0554;	0.0465;	0.0534;
wR2 [I >2σ(I)]	0.1171	0.0963	0.1208
CCDC	2075692	2075693	2075694

Magnetic properties

Magnetic susceptibility data for complexes **1-3** were collected at 193 Oe (2-30 K) and 3000 Oe (2-300 K). Field dependent phenomena were not observed. The χT product under applied dc magnetic field in the temperature range of 2 to 300 K for complexes **1–3** is shown in Figure 7a. The dc magnetic measurements reveal a room temperature χT value of 66, 64 and 20 cm^3 K mol^{-1} for complexes **1–3** respectively, which are in good agreement with the expected value of 68, 68 and 22 cm^3 K mol^{-1} for four Co^{II} and four Ln^{III} ions, taking into account the strong spin-orbit coupling for Dy^{III}, Ho^{III} and Yb^{III}. As temperature decreases, the magnetic susceptibility value is nearly constant until a temperature of 100 K. Below this temperature, a marked decrease is observed for all complexes, as expected due to the depopulation of the M_J sublevels of the Ln^{III} and Co^{II} centers. An increase in the χT values is observed below 15 K for all complexes, being this increase more pronounced for **1** (Dy) and **2** (Ho) analogues. This increase should be attributed to ferromagnetic coupling between the metal centers of

the Co_4Ln_4 complexes. A simple Curie Weiss analysis yields Curie constant of 66 cm^3/mol for **1**, 64 cm^3/mol for **2** and 20 cm^3/mol for **3**. The Weiss constant for all samples is small and yields values of −2.13 K for **1**, −1.99 K for **2** and −5.12 K for **3** (Figure 7b). The values are small, as expected for lanthanoid complexes, that usually display weak magnetic coupling to other 4f or 3d ions. The negative sign indicates overall antiferromagnetic behavior. Part of the magnetic coupling can be dipolar in origin, as usual for Ln ions. The Dy_2O_2 diamonds observed in the crystal structure with Dy–O–Dy angles between 102° and 103° and the Co–O–Dy angles between 94° and 109° can lead to both ferromagnetic or antiferromagnetic coupling. Dipolar contributions are usually important for Dy^{III} complexes, and a simple model relates the dipolar contribution to the magnetic coupling with the distances between the metal ion centers and the angle between the anisotropy axes. We used Magellan[62] to calculate the anisotropy axes on the Dy ions of complex **1**, as shown in Figure 7d. The dipolar interactions between each Dy^{III} ion with its first neighbors were calculated, within the effective Hamiltonian, with the expression $Jdip = \frac{\mu o g_z^{*2} \mu_B^2}{8\pi r^3}(3cos^2\theta - 1)$ taking into account the Dy···Dy separation of r and the relative orientation of the anisotropy axes of the considered Dy ions, as calculated by Magellan package. The results, summarized in Table 2, show a weak ferromagnetic contribution to the magnetic exchange by the dipolar interaction between the Dy^{III} ions in **1**. The collinearity of the anisotropy axes on all four Dy^{III} ions is responsible for this ferromagnetic contribution and it provides the molecule with axial anisotropy, a requirement for an SMM.

Table 2. Dipolar contribution to the magnetic coupling

Dy···Dy	Dy···Dy distance (Å)	Angle (radians)	J*dip/k_B (K)
1-2	3.661	0.795	1.020
3-4	3.685	0.706	1.569
1-3	7.955	0.474	0.291
1-4	7.247	0.855	0.081
2-3	7.202	0.779	0.148
2-4	5.669	0.203	1.099

The molar magnetization (M) *vs* field (H) plot for the complexes **1–3** is shown in Figure 7c, which shows a rapid increase at low field followed by a gradual increase which reaches at 28, 28 and 15 Nμ_B at

temperature 2K at 5 T for complexes **1–3** respectively, indicating a strong magnetic interaction, another requirement for an SMM. It is worth noting here that the ligand anions persuade a rotation of one Co_2Ln_2 unit with respect to the other, this is clearly shown in Figure 5. This greatly affects the magnetic properties of complex **1**. One Dy^{III} ion at the top of Co_2Ln_2 unit, Dy1 in Table 2, is further apart from the bottom Co_2Ln_2 unit than Dy2. Therefore, even though in each Co_2Ln_2 unit the Dy···Dy coordination and bridging are the same, the Dy^{III} ions in the Dy_2O_2 diamond cores were not magnetically equivalent.

Given the anisotropic nature of the Dy^{III} in **1**, and that there is a non-diamagnetic ground state, we decided to explore the dynamic magnetic properties of the complexes, with a focus on the Dy analogue **1**. Alternating current (ac) magnetic susceptibility measurements were performed to investigate the slow relaxation of the magnetization. Data were collected for all samples at temperatures between 1.8 and 10 K, and with frequencies of the oscillating ac field between 1 and 1488 Hz. For all cases, data with and without applied dc field were collected but only

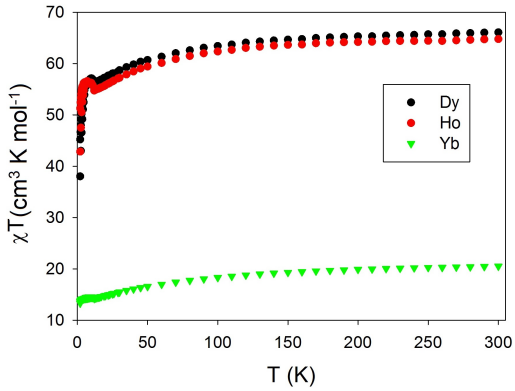

(c)

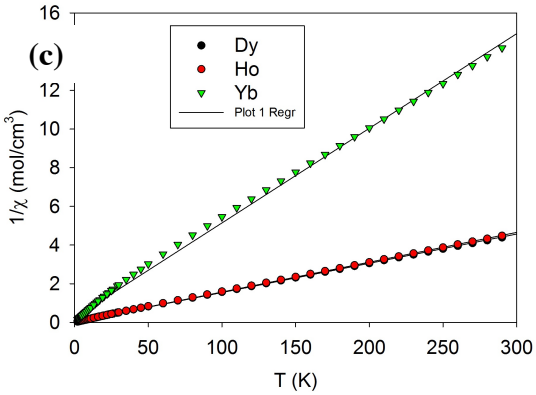

(d)

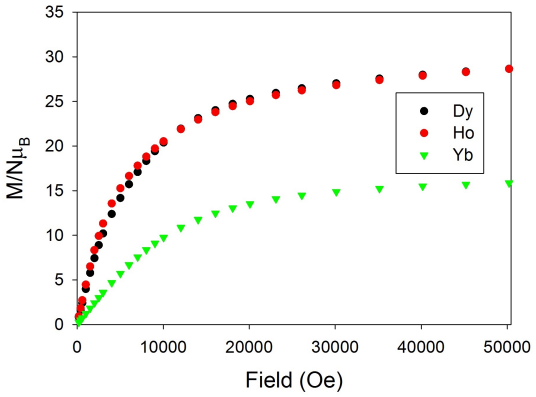

(a)

(b)

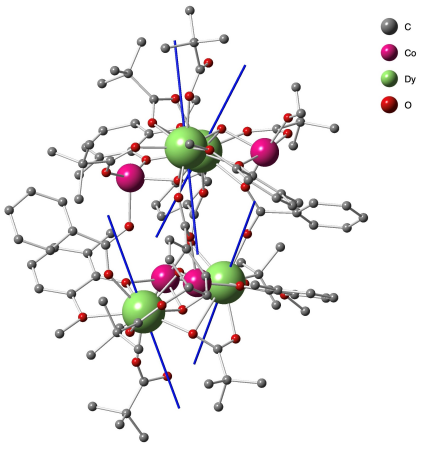

Figure 7. (a) Plot of χT product *vs* T for **1–3** at applied fields of 193 Oe (2-30 K) and 3000 Oe (2-300 K); (b) Curie-Weiss plots for **1–3**, see text for fitting parameters; (c) anisotropy axes on the Dy^{III} of **1**, as calculated by Magellan; (d) magnetization *vs* field plot for **1–3** at 2 K

for complex **1** an out-of-phase ac magnetic susceptibility signal was observed without an applied dc field. When a dc field was applied to collect ac data, significant changes were not observed for any of the compounds. For complex **1**, the only analogue with an ac peak without an applied dc field, a significant shift of the signal was not observed when a dc magnetic field was applied, so the ac data reported has been collected without applied dc field. The plot of temperature dependent and frequency dependent out-of-phase (χ″) susceptibility signals shown in Figure 8a and 8b are characteristic of slow relaxation of magnetization in complex **1**. The magnetization relaxation time (τ) is extracted from the temperature dependent data and fitted to the simple Arrhenius model as a plot of ln (1/τ) vs 1/T as shown in Figure 8c. The values extracted from the linear Arrhenius fit [$\tau = \tau_0 \exp(U_{eff}/k_B T)$] were a relaxation time, $\tau_0 = 1.51\times 10^{-6}$ s and an effective energy barrier, $U_{eff} = 12.5$ K. At the lowest possible temperature in a commercial SQUID (1.8 K), a hysteresis loop of magnetization *vs* magnetic field was not observed for the complex **1**. A Cole-Cole plot is used to study the distribution of the relaxation process (χ″ vs χ′) which is shown in Figure 8d between 1.8 K and 2.7 K. The data was fitted using the Debye model[63] (solid lines, fitting values in SI Table S6) to obtain an average alpha value of 0.05, in agreement with a single relaxation process with a narrow distribution of energy barriers. Since the Ho and Yb analogues **2** and **3** do not display SMM character, it is clear that the contribution to the molecular magnetic anisotropy of Dy ions is a key factor for the SMM properties in **1**. This is not always the case for cobalt(II)-4f complexes,[35] but in this series of complexes it is a combination of a ground state magnetic moment and the collinearity of the anisotropy axes on the four Dy ions that led to the observed SMM behavior.

(a) **(b)**

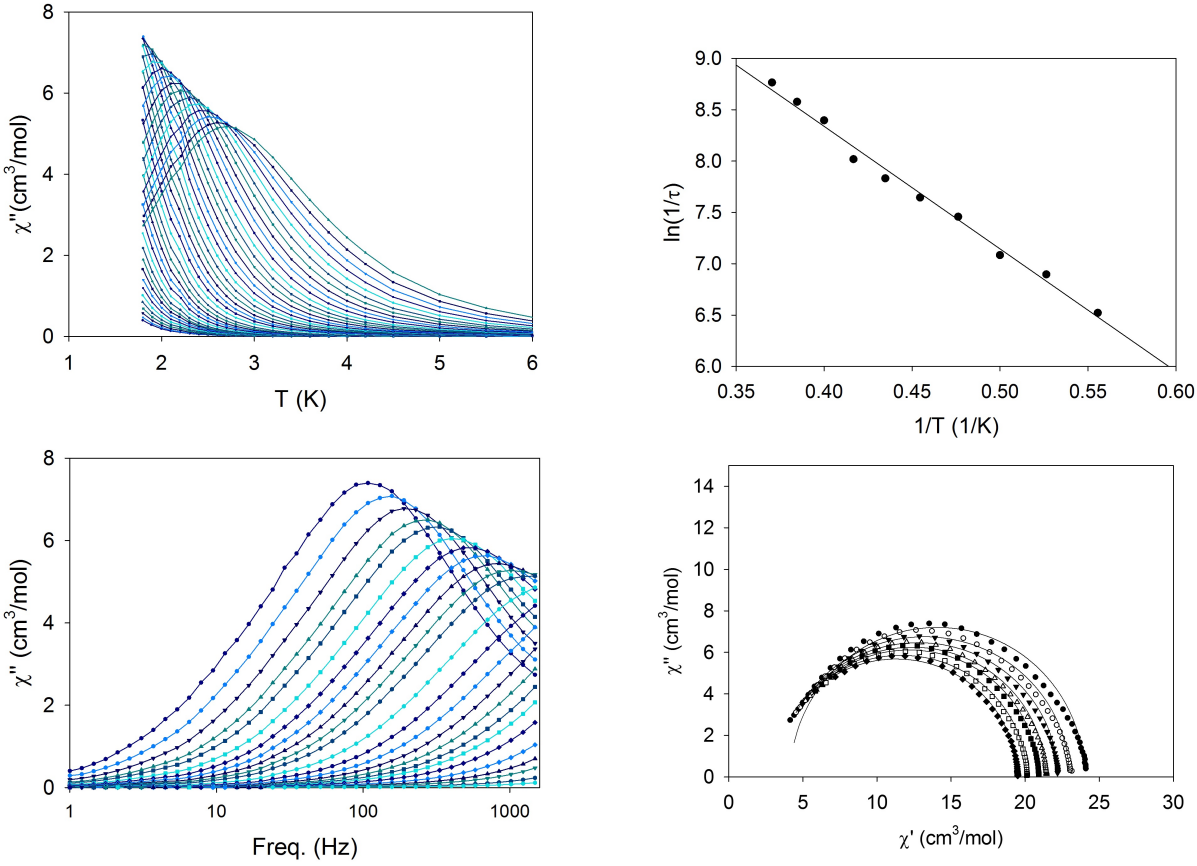

(c)

(d)

Figure 8. Ac magnetic susceptibility data for complex frequencies between 1 Hz and 1488 Hz, and temperatures between 1.8 K and 6 K, without an applied dc field: (a) χ'' *vs* T plot, (b) χ'' *vs* freq. plot with a logarithmic frequency scale; (c) Arrhenius plot and (d) Argand plot for the dynamic ac magnetic susceptibility data between 1.8 K and 2.7 K

The core found in these $[Co_2Ln_2]_2$ complexes is a well-known structure found for many transition metal complexes, known as defective dicubane. Many $Mn(II)_2Mn(III)_2$ complexes have been reported with this core that are SMMs, a review of their properties and structures can be found in Aromi and Brechin's review.[1] In the complexes reported here the

tetranuclear units are linked by the ligand into octanuclear complexes. For transition metals there are also examples of this kind of dimers, as those reported by Sañudo et al for Mn and Fe.[2,3] The coupling between units is usually weak, since the ligands are large enough to accommodate two tetranuclear complexes in close proximity. However, the compounds reported here are a very special case due to the rotation imposed by the short ligands. The rotation or twist, illustrated in Figures 5 and 7(c), between the two Co_2Dy_2 fragments makes both Dy ions in the Dy_2O_2 diamond units magnetically non-equivalent. This further complicates the magnetic analysis. As reviewed by Rosado and Sañudo, most Co_2Ln_2 defective dicubane complexes that report SMM properties contain Co(III) and are good SMMs.[4] Very good examples are reported by Funes *et al*.[5] and Langley *et al*., where they show complexes with large energy barriers,[6,7] and independent Dy sites that lead to a distribution of barriers.[8] However, the complexes reported here contain the known defective dicubane core but the oxidation state of Cobalt is Co(II), not Co(III). Thus the Co(II) ions contribute to the magnetic properties of the resulting complex, but they fail to provide the extra boost needed to achieve better SMMs.

New references:

(1) Aromí, G.; Brechin, E. K. Synthesis of 3 d Metallic Single-Molecule Magnets. In *Structure and Bonding*; Springer-Verlag: Berlin, 2006; pp. 1–67.

(2) Sañudo, E. C.; Cauchy, T.; Ruiz, E.; Laye, R. H.; Roubeau, O.; Teat, S. J.; Aromí, G. Molecules Composed of Two Weakly Magnetically Coupled [MnIII4] Clusters. *Inorg. Chem.* **2007**, *46*, 9045–9047.

(3) Sañudo, E. C.; Uber, J. S.; Pons Balagué, A.; Roubeau, O.; Aromí, G. Molecular [(Fe 3)-(Fe 3)] and [(Fe 4)- (Fe 4)] Coordination Cluster Pairs as Single or Composite Arrays. *Inorg. Chem.* **2012**, *51*, 8441–8446.

(4) Rosado Piquer, L.; Sañudo, E. C. Heterometallic 3d–4f Single-Molecule Magnets. *Dalt. Trans.* **2015**, *44*, 8771–8780.

(5) Funes, A. V; Carrella, L.; Rentschler, E.; Alborés, P. {CoIII2DyIII2} Single Molecule Magnet with Two Resolved Thermal Activated Magnetization Relaxation Pathways at Zero Field. *Dalt. Trans.* **2014**, *43*, 2361–2364.

(6) Langley, S. K.; Chilton, N. F.; Moubaraki, B.; Murray, K. S. Single-Molecule Magnetism in Three Related {CoIII 2DyIII 2}-Acetylacetonate Complexes with Multiple Relaxation Mechanisms Stuart. *Inorg. Chem.* **2013**, *52*, 7183–7192.

(7) Langley, S. K.; Ungur, L.; Chilton, N. F.; Moubaraki, B.; Chibotaru, L. F.; Murray, K. S. Single-Molecule Magnetism in a Family of {CoIII 2DyIII 2} Butterfly Complexes: Effects of Ligand Replacement on the Dynamics of Magnetic Relaxation. *Inorg. Chem.* **2014**, *53*, 4303–4315.

(8) Langley, S. K.; Chilton, N. F.; Ungur, L.; Moubaraki, B.; Chibotaru, L. F.; Murray, K. S. Heterometallic Tetranuclear [LnIII 2CoIII 2] Complexes Including Suppression of Quantum Tunneling of Magnetization in the [DyIII 2CoIII 2] Single Molecule Magnet. *Inorg. Chem.* **2012**, *51*, 11873–11881.

Conclusions

Initial focus on the stepwise assembly of binuclear to tetranuclear to octanuclear aggregates from the use of multiple ions within binucleating ligand anion scaffold has been shifted on to the use of lanthanide ions on account of their larger anisotropies and larger spin values in probing their SMM behavior. Recent studies like the work reported in this paper have demonstrated that coordination chemistry and structural modification can be exploited to manipulate magnetic properties of 4f ion bearing species to maximize energy barrier heights and minimize under barrier relaxation processes such as QTM. The reported work exposed several characteristic

observations: (a) the importance and presence of Ln^{III} ions capable of showing a higher coordination number nicely matched with varying types and numbers of carboxylate coordination; (b) placement of different bridging entities attaching two different coordination spheres lead to distortions around Co^{II} environments for synergistic and cooperative clipping of Co^{II} and Ln^{III} ions; (c) trapping of two different categories of metal ions in two different coordination pockets of single ligand backbone was responsible for the distortions of both the polyhedral types; (d) the presence of terminal carboxylato ends of the organic ligands were available for linking two Co_2Ln_2 partial dicubane units. This is a new report of such drum-shaped octanuclear Co^{II}-Ln^{III} complexes established from the fascinating arrangements of endogenous and exogenous carboxylate anions. We have successfully validated the use and involvement of hydrolysis limiting and structure supporting ligand anions for the desired aggregation processes. The work also demonstrated that the chosen organic Schiff base is most efficient to limit the hydrolysis at the 4f ion centers and controlled the condensation pathway by trapping the Co_4Ln_4 species as final stable isolable products. The reported synergistic coordination chemistry of transition and lanthanide metal ions, is full of potential for further synthetic modification and discovery of newer coordination aggregates through incorporation of appropriate numbers of 3d and 4f ions. From the dynamic participation of the transition metal ions, the template effects of bridging phenoxido group of the ligand anion and the availability of the *in situ* generated and 4f ion bound HO^- ions are important in availing the reaction products in ambient condition.

The magnetic properties of complexes **1–3** have been examined in detail. Complex **1**, the Dy analogue, is shown to be a new example of SMM. The $\{Co_2Ln_2\}_2$ core contains a fairly common structure of carboxylato connected two Ln_2O_2 diamond units. The cobalt(II) ions did not provide the central $\{M_2O_2\}$ cores, but at the tips of the fragments, resulting in two fairly well separated ligand anion bound cobalt(II) ions, nearly magnetically independent. However, structure of the ligand in the complex leads to a twisting between the two Co_2Dy_2 fragments that makes both Dy ions in the Dy_2O_2 diamond units magnetically non-equivalent.

ASSOCIATED CONTENT

Supporting Information

The Supporting Information is available free of charge at

Tables S1–S6, Figures S1–S4 (PDF)

AUTHOR INFORMATION

Corresponding Author

Debashis Ray

orcid.org/0000-0002-4174-6445; Phone: (+91) 3222-283324;

Email: dray@chem.iitkgp.ac.in; Fax: (+91) 3222-82252

Notes

The authors declare no competing financial interest.

ACKNOWLEDGMENT

M.B. would like to acknowledge University Grants Commission (UGC) New Delhi, India for financial support. We also would like to acknowledge the DST, New Delhi, India, for providing the single-crystal X-ray diffractometer facility at the Department of Chemistry, IIT Kharagpur, under its FIST program. E.C.S. would like to acknowledge the financial support from Spanish Governement Ministerio de Ciencia y Universidades, grant number PGC2018-098630-B-I00.

REFERENCES

(1) Sharples, J. W.; Collison. D. The coordination chemistry and magnetism of some 3d–4f and 4f amino-polyalcohol compounds. *Coord. Chem. Rev.* **2014**, *260*, 1– 20.

(2) Liu, K.; Shi, W.; Cheng, P. Toward heterometallic single-molecule magnets: Synthetic strategy, structures and properties of 3d–4f discrete complexes. *Coord. Chem. Rev.* **2015**, *289–290*, 74–122.

(3) Yadav, R.; Hossain, M.-E.; Paramban, R.-P.; Simler, T.; Schoo, C.; Wang, J.; Deacon, J. B.; Junk, P. C.; Roesky, P.W. 3d–4f heterometallic complexes by the reduction of transition metal carbonyls with bulky Ln^{II} amidinates. *Dalton Trans.* **2020**, *49*, 7701-7707.

(4) Andruh, M.; Costes, J.-P.; Diaz, C.; Gao, S. 3d-4f Combined Chemistry: Synthetic Strategies and Magnetic Properties. *Inorg. Chem.* **2009**, *48*, 3342-3359.

(5) Chen, Q.-Y.; Luo, Q.-H.; Hu, X.-L.; Shen, M.-C.; Chen, J.-T. Heterodinuclear Cryptates $[EuML(dmf)](ClO_4)_2$(M = Ca, Cd, Ni, Zn):Tuning the Luminescence of Europium(III) through the Selection of the Second Metal Ion. *Chem.–Eur. J.* **2002**, *8*, 3984–3990

(6) Chen, S.; Mereacre, V.; Prodius, D.; Kostakis, G. K.; Powell, A. K. Developing a “Highway Code” To Steer the Structural and Electronic Properties of Fe^{III}/Dy^{III} Coordination Clusters. *Inorg. Chem.* **2015**, *54*, 3218–3227.

(7) (a) Griffiths, K.; Tsipis, A. C.; Kumar, P.; Townrow, O. P. E.; Abdul-Sada, A.; Akien, G. R.; Baldansuren, A.; Spivey A. C.; Kostakis, G. E. 3d/4f

Coordination Clusters as Cooperative Catalysts for Highly Diastereoselective Michael Addition Reactions. *Inorg. Chem.* **2017**, *56*, 9563–9573; (b) K. Griffiths, P. Kumar, G. R. Akien, N. F. Chilton, A. Abdul-Sada, G. J. Tizzard, S. J. Coles, and G. E. Kostakis. Tetranuclear Zn/4f coordination clusters as highly efficient catalysts for Friedel–Crafts alkylation. *Chem. Commun.* **2016**, *52*, 7866–7869; (c) K. Griffiths, P. Kumar, J. D. Mattock, A. Abdul-Sada, M. B. Pitak, S. J. Coles, O. Navarro, A. Vargas, and G. E. Kostakis. Efficient $Ni^{II}_2Ln^{III}_2$ Electrocyclization Catalysts for the Synthesis of trans-4,5-Diaminocyclopent-2-enones from 2-Furaldehyde and Primary or Secondary Amines. *Inorg. Chem.* **2016**, *55*, 6988–6994.

(8) Kettles, F. J.; Milway, V. A.; Tuna, F.; Valiente, R.; Thomas, L. H.; Wernsdorfer, W; Ochsenbein, S. T.; Murrie, M. Exchange Interactions at the Origin of Slow Relaxation of the Magnetization in $\{TbCu_3\}$ and $\{DyCu_3\}$ Single-Molecule Magnets. *Inorg. Chem.* **2014**, *53*, 8970–8978.

(9) Zaleski, C. M.; Depperman, E. C.; Kampf, J. W.; Kirk, M. L.; Pecoraro, V. L. Synthesis, Structure, and Magnetic Properties of a Large Lanthanide–Transition-Metal SingleMolecule Magnet. *Angew. Chem. Int. Ed.* **2004**, *43*, 3912–3914.

(10) Rosado Piquer, L.; Sañudo, E. C. Heterometallic 3d–4f single-molecule magnets. *Dalton Trans.* **2015**, *44*, 8771–8780.

(11) Vignesh, K. R.; Soncini, A.; Langley, S. K.; Wernsdorfer, W.; Murray, K. S.; & Rajaraman, G. Ferrotoroidic ground state in a heterometallic $\{Cr^{III}Dy^{III}_6\}$ complex displaying slow magnetic relaxation. *Nature Commun.* **2017**, 1023(1-12).

(12) Alexandropoulos, D. I.; Poole, K. M.; Cunha-Silva, L.; Sheikh, J.-A.; Wernsdorfer, W.; Christou, G.; Stamatatos, T. C. A family of 'windmill'-like $\{Cu_6Ln_{12}\}$ complexes exhibiting single-molecule magnetism behavior and large magnetic entropy changes. *Chem. Commun.* **2017**, *53*, 4266–4269.

(13) Pedersen, K. S.; Ariciu, K.-M.; McAdams, S.; Weihe, H.; Bendix, J.; Tuna, F.; Piligkos, S. Toward Molecular 4f Single-Ion Magnet Qubits, *J. Am. Chem. Soc.* **2016**, *138*, 5801–5804.

(14) Urdampilleta, M.; Klyatskaya, S.; Cleuziou, J.-P.; Ruben, M.; Wernsdorfer, W. Supramolecular spin valves. *Nat. Mater.* **2011**, *10*, 502–506.

(15) Bogani, L.; Wernsdorfer, W. Molecular spintronics using single molecule magnets. *Nat. Mater.* **2008**, *7*, 179–186.

(16) Rocha, A. R.; García-suárez, V. M.; Bailey, S. W.; Lambert, C. J.; Ferrer, J.; Sanvito, S. Towards molecular spintronics. *Nat. Mater.* **2005**, *4*, 335–339.

(17) Sessoli, R.; Gatteschi, D.; Caneschi, A.; Novak, M. A. Magnetic Bistability in a Metal-Ion Cluster. *Nature*, **1993**, *365*, 141-143.

(18) Leuenberger, M. N.; Loss, D. Quantum computing in molecular magnets. *Nature*, **2001**, *410*, 789-793.

(19) Coronado, E.; Epsetin, A. J. Molecular spintronics and quantum computing. *J. Mater. Chem.* **2009**, *19*, 1670–1671.

(20) Zheng, Y.-Z.; Evangelisti, M.; Tuna, F.; Winpenny, R. E. P. Co–Ln Mixed-Metal Phosphonate Grids and Cages as Molecular Magnetic Refrigerants. *J. Am. Chem.Soc.* **2012**, *134*, 1057–1065.

(21) Liu, C.-M.; Zhang, D.-Q.; Zhu, D.-B. Hexanuclear $[Ni_2Ln_4]$ clusters exhibiting enhanced magnetocaloric effect and slow magnetic relaxation. *RSC Adv.* **2014**, *4*, 53870–53876.

(22) Karotsis, G.; Kennedy, S.; Teat, S. J.; Beavers, C. M.; Fowler, D. A.; Morales, J. J.; Evangelisti, M.; Dalgarno, S. J.; Brechin, E. K. $[Mn^{III}_4Ln^{III}_4]$ Calix[4]arene Clusters as Enhanced Magnetic Coolers and Molecular Magnets. *J. Am. Chem. Soc.* **2010**, *132*, 12983-12990.

(23) Rinehart, J. D.; Fang, M.; Evans, W. J.; Long, J. R. Strong exchange and magnetic blocking in N_2^{3-}-radical-bridged lanthanide complexes. *Nat. Chem.* **2011**, *3*, 538–542.

(24) Maity, S.; Mondal, A.; Konar, S.; Ghosh, A. The role of 3d–4f exchange interaction in SMM behaviour and magnetic refrigeration of carbonato bridged $Cu^{II}_2Ln^{III}_2$ (Ln = Dy, Tb and Gd) complexes of an unsymmetrical N_2O_4 donor ligand. *Dalton Trans.* **2019**, *48*, 15170–15183.

(25) Dolai, M.; Ali, M.; Titiš, J.; Boča, R. Cu(II)–Dy(III) and Co(III)–Dy(III) based single molecule magnets with multiple slow magnetic relaxation processes in the Cu(II)–Dy(III) complex. *Dalton Trans.* **2015**, *44*, 13242–13249.

(26) Bhanja, A.; Herchel, R.; Trávníček, Z.; Ray, D. Two Types of Hexanuclear Partial Tetracubane $[Ni_4Ln_2]$ (Ln = Dy, Tb, Ho) Complexes of Thioether-Based Schiff Base Ligands: Synthesis, Structure, and Comparison of Magnetic Properties. *Inorg. Chem.* **2019**, *58*, 12184–12198.

(27) Vallejo, J.; Castro, I.; Ruiz-García, R.; Cano, J.; Julve, M.; Lloret, F.; Munno, G.-D.; Wernsdorfer, W.;

Pardo, E. Field-Induced Slow Magnetic Relaxation in a Six-Coordinate Mononuclear Cobalt(II) Complex with a Positive Anisotropy. *J. Am. Chem. Soc.* **2012**, *134*, 15704–15707.

(28) Mondal, K. C.; Sundt, A.; Lan, Y.; Kostakis, G. E.; Waldmann, O.; Ungur, L.; Chibotaru, L. F.; Anson, C. E.; Powell, A. K. Coexistence of Distinct Single-Ion and Exchange-Based Mechanisms for Blocking of Magnetization in a $Co^{II}_2Dy^{III}_2$ Single-Molecule Magnet. Angew. *Chem. Int. Ed.* **2012**, *51*, 7550 –7554.

(29) Peng, Y.; Mereacre, V.; Anson, C. E.; Powell, A. K. The role of coordinated solvent on Co(II) ions in tuning the single molecule magnet properties in a $\{Co^{II}_2Dy^{III}_2\}$ system. *Dalton Trans.* **2017**, *46*, 5337–5343.

(30) Ferbinteanu, M.; Kajiwara, T.; Choi, K. Y.; Nojiri, H.; Nakamoto, A.; Kojima, N.; Cimpoesu, F.; Fujimura, Y.; Takaishi, S.; Yamashita, M. A binuclear Fe(III)Dy(III) single molecule magnet. Quantum effects and models. *J. Am. Chem. Soc.* **2006**, *128*, 9008–9009.

(31) Lin, P.-H.; Burchell, T. J.; Ungur, L.; Chibotaru, L. F.; Wernsdorfer, W.; Murugesu, M. A Polynuclear Lanthanide Single-Molecule Magnet with a Record Anisotropic Barrier. *Angew. Chem.*, **2009**, *121*, 9653; *Angew. Chem. Int. Ed.* **2009**, *48*, 9489–9492.

(32) Langley, S. K.; Wielechowski, D. P.; Vieru, V.; Chilton, N. F.; Moubaraki, B.; Abrahams, B. F.; Chibotaru, L. F.; Murray, K. S. A $\{Cr^{III}_2Dy^{III}_2\}$ Single-Molecule Magnet: Enhancing the Blocking Temperature through 3d Magnetic Exchange. *Angew. Chem. Int. Ed.* **2013**, *52*, 12014 –12019.

(33) Li, X.-L.; Min, F.-Y.; Wang, C.; Lin, S.-Y.; Liu, Z.; Tang, J. Utilizing 3d–4f Magnetic Interaction to Slow the Magnetic Relaxation of Heterometallic Complexes. *Inorg. Chem.* **2015**, *54*, 4337–4344.

(34) Costes, J.-P.; Vendier, L.; Wernsdorfer, W. Structural and magnetic studies of original tetranuclear Co^{II}–Ln^{III} complexes (Ln^{III} = Gd, Tb, Y). *Dalton Trans.* **2011**, *40*, 1700–1706.

(35) Rosado Piquer, L.; Dey, S.; Castilla-Amorós, L.; Teat, S. J.; Cirera, J.; Rajaraman, G.; Sañudo, E. C. Microwave assisted synthesis of heterometallic 3d–4f M_4Ln complexes. *Dalton Trans.* **2019**, *48*, 12440–12450.

(36) Zhao, X.; Li, G.; Ma, J.; Liu, W. Two Octanuclear $\{Cu_4Ln_4\}$ (Ln = Dy or Tb) Complexes with a Butterfly-Shaped Unit Exhibiting Zero-Field Single-Molecule Magnet Behavior. *Inorg. Chem.* **2020**, *59*, 2328–2336.

(37) Hussain, B.; Savard, D.; Burchell, T. J.; Wernsdorfer, W.; Murugesu, M. Linking high anisotropy Dy_3 triangles to create a Dy_6 single-molecule magnet. *Chem. Commun.* **2009**, *9*, 1100–1102.

(38) Zou, H.-H.; Sheng, L.-B.; Liang, F.-P.; Chen, Z.-L.; Zhang, Y.-Q. Experimental and theoretical investigations of four 3d–4f butterfly single-molecule magnets. *Dalton Trans.* **2015**, *44*, 18544–18552.

(39) Ke, H.; Zhao, L.; Guo, Y.; Tang, J. Syntheses, Structures, and Magnetic Analyses of a Family of Heterometallic Hexanuclear $[Ni_4M_2]$ (M = Gd, Dy, Y) Compounds: Observation of Slow Magnetic Relaxation in the Dy^{III} Derivative. *Inorg. Chem.* **2012**, *51*, 2699–2705.

(40) Griffiths, K.; Novitchi, G.; Kostakis, G. E. Synthesis, Characterization, Magnetic Properties, and Topological Aspects of Isoskeletal Heterometallic Hexanuclear $Co^{II}_4Ln^{III}_2$ Coordination Clusters Possessing 2,3,4M6–1 Topology. *Eur. J. Inorg. Chem.* **2016**, *17*, 2750–2756.

(41) Jiang, L.; Liu, B.; Zhao, H.-W.; Tian, J.-L.; Liu, X.; Yan, S.-P. Compartmental ligand approach for constructing 3d–4f heterometallic $[Cu^{II}_5Ln^{III}_2]$ clusters: synthesis and magnetostructural properties. *CrystEngComm.* **2017**, *19*, 1816–1830.

(42) Goura, J.; Guillaume, R.; Rivière, E.; Chandrasekhar, V. Hexanuclear, Heterometallic, Ni_3Ln_3 Complexes Possessing O-Capped Homo- and Heterometallic Structural Subunits: SMM Behavior of the Dysprosium Analogue. *Inorg. Chem.* **2014**, *53*, 7815–7823.

(43) Baskar, V.; Gopal, K.; Helliwell, M.; Tuna, F.; Wernsdorfer, W.; Winpenny, R. E. P. 3d–4f Clusters with large spin ground states and SMM behavior. *Dalton Trans.* **2010**, *39*, 4747–4750.

(44) Zheng, Y.-Z.; Evangelisti, M.; Winpenny, R. E. P. Co–Gd phosphonate complexes as magnetic refrigerants. *Chem. Sci.* **2011**, *2*, 99–102.

(45) Mereacre, V.; Ako, A. M.; Clerac, R.; Wernsdorfer, W.; Hewitt, I. J.; Anson, C. E.; Powell, A. K. Heterometallic $[Mn_5\text{-}Ln_4]$ Single-Molecule Magnets with High Anisotropy Barriers. *Chem.–Eur. J.* **2008**, *14*, 3577–3584.

(46) Gao, Y.; Xu, G.-F.; Zhao, L.; Tang, J.; Liu, Z. Observation of Slow Magnetic relaxation in Discrete Dysprosium Cubane. *Inorg. Chem.* **2009**, *48*, 11495–11497.

(47) Peng, J.-B.; Zhang, Q.-C.; Kong, X.-J.; Zheng, Y,-Z.; Ren, Y.-P.; Long, L.-S.; Huang, R.-B.; Zheng, L.-S.; Zheng, Z. High-Nuclearity 3d–4f Clusters as

Enhanced Magnetic Coolers and Molecular Magnets. *J. Am. Chem. Soc.* **2012**, *134*, 3314–3317.

(48) Guarda, E.; Bader, K.; Slageren, J. V.; Alborés, P. $\{Ni^{II}_8Ln^{III}_6\}$ (Ln = Gd, Dy) rod-like nano-sized heteronuclear coordination clusters with a double carbonate bridge skeleton and remarkable MCE behaviour. *Dalton Trans.* **2016**, *45*, 8566–8572.

(49) Bag, P.; Rastogi, C. K.; Biswas, S.; Sivakumar, S.; Mereacre, V.; Chandrasekhar, V. Homodinuclear lanthanide $\{Ln_2\}$ (Ln = Gd, Tb, Dy, Eu) complexes prepared from an o-vanillin based ligand: luminescence and single-molecule magnetism behavior. *Dalton Trans.* **2015**, *44*, 4328–4340.

(50) Ke, H.; Gamez, P.; Zhao, L.; Xu, G.-F.; Xue, S.; Tang, J. Magnetic Properties of Dysprosium Cubanes Dictated by the M-O-M Angles of the $[Dy_4(\mu_3\text{-}OH)_4]$ Core. *Inorg. Chem.* **2010**, *49*, 7549–7557.

(51) She, S.; Chen, Y.; Zaworotko, M. J.; Liu, W.; Cao, Y.; Wu, J.; Li, Y. Synthesis, structures and magnetic properties of a family of nitrate-bridged octanuclear $[Na_2Ln_6]$ (Ln = Dy, Tb, Gd, Sm) complexes. *Dalton Trans.* **2013**, *42*, 10433–10438.

(52) She, S.; Li, Y.; Li, W. Two 3d-4f double helical chains including $[Dy_2M_2]_n$ (M = Ni^{II} and Co^{II}) cores exhibiting slow magnetic relaxation. *Dalton Trans.* **2016**, *45*, 10830 –10835.

(53) AromÌ, G.; Batsanov, A. S.; Christian, P.; Helliwell, M.; Parkin, A.; Parsons, S.; Smith, A. A.; Timco, G. A.; Winpenny, R. E. P. Synthetic and Structural Studies of Cobalt ± Pivalate Complexes. *Chem.–Eur. J.* **2003**, *9*, 5142–5161.

(54) Yuhua, F.; Caifeng, B.; Jinying, L. Synthesis and characterization of UO_2(II) and Th(IV) binuclear complexes with o-vanillylidene anthranilic acid. *J. Radioanal. Nucl. Chem.* **2002**, *254*, 641–644.

(55) *SAINT, SMART and XPREP*; Siemens Analytical X-ray, Instruments Inc., Madison, WI, 2003.

(56) Sheldrick, G. M. SADABS Software for Empirical Absorption Correction; Institute fur Anorganische Chemieder Universitat, University of Göttingen, Göttingen, Germany, 1999–2003.

(57) Sheldrick, G. M. *SHELXS-2014, Program for Crystal Structure Solution*; University of Göttingen, Göttingen, Germany, 2014.

(58) Sheldrick, G. M. Crystal Structure Refinement with SHELXL. *Acta Crystallogr., Sect. A: Found. Crystallogr.* **2008**, *64*, 112–122.

(59) Dolomanov, O. V.; Bourhis, L. J.; Gildea, R. J.; Howard J. A. K.; Puschmann, H. OLEX2: a complete structure solution, refinement and analysis program. *J. Appl. Crystallogr.* **2009**, *42*, 339–341

(60) Farrugia, L. J. *POV-Ray - 3.5*; University of Glasgow, Glasgow, U.K., 2003.

(61) (a) Casanova, D.; Cirera, J.; Liunell, M.; Alemany, P.; Avnir, D.; Alvarez, S. Minimal Distortion Pathways in Polyhedral Rearrangements. *J. Am. Chem. Soc.* **2004**, *126*, 1755–1763; (b) Alvarez, S.; Alemany, P.; Casanova, D.; Cirera, J.; Llunell, M.; Avnir, D. Shape maps and polyhedral interconversion paths in transition metal chemistry. *Coord. Chem. Rev.* **2005**, *249*, 1693–1708.

(62) Chilton, N. F.; Collison, D.; McInnes, E. J. L.; Winpenny, R. E. P.; Soncini, A. An electrostatic model for the determination of magnetic anisotropy in dysprosium complexes, *Nature Commun.* **2013**, *4*, 2551(1-7).

(63) Cole, K. S.; Cole, R. H. Dispersion and Absorption in Dielectrics I. Alternating Current Characteristics. *J. Chem. Phys.* **1941**, *9*, 341-351.

TOC Synopsis

Four Schiff base ligands [(2-((2-hydroxy-3-methoxybenzylidene)amino)benzoic acid), H_2L] have been utilized for the spontaneous self-assembly of Co_4Ln_4 coordination aggregates. Terminal carboxy ends of the ligand anion showed inter tetrameric coordination and Dy(III) analogue showed SMM behavior in absence of external magnetic field, with U_{eff} of 12.5 K.